**SANDIA REPORT** 

SAND2021-14544 Printed November 2021



# Transmitted wave measurements in cold sprayed materials under dynamic compression

Chad A. McCoy, Brittany A. Branch, and Andrew Vackel

Prepared by Sandia National Laboratories Albuquerque, New Mexico 87185 and Livermore, California 94550 Issued by Sandia National Laboratories, operated for the United States Department of Energy by National Technology & Engineering Solutions of Sandia, LLC.

**NOTICE:** This report was prepared as an account of work sponsored by an agency of the United States Government. Neither the United States Government, nor any agency thereof, nor any of their employees, nor any of their contractors, subcontractors, or their employees, make any warranty, express or implied, or assume any legal liability or responsibility for the accuracy, completeness, or usefulness of any information, apparatus, product, or process disclosed, or represent that its use would not infringe privately owned rights. Reference herein to any specific commercial product, process, or service by trade name, trademark, manufacturer, or otherwise, does not necessarily constitute or imply its endorsement, recommendation, or favoring by the United States Government, any agency thereof, or any of their contractors or subcontractors. The views and opinions expressed herein do not necessarily state or reflect those of the United States Government, any agency thereof, or any of their contractors.

Printed in the United States of America. This report has been reproduced directly from the best available copy.

Available to DOE and DOE contractors from

U.S. Department of Energy Office of Scientific and Technical Information P.O. Box 62 Oak Ridge, TN 37831

Telephone: (865) 576-8401 Facsimile: (865) 576-5728 E-Mail: reports@osti.gov

Online ordering: <a href="http://www.osti.gov/scitech">http://www.osti.gov/scitech</a>

Available to the public from

U.S. Department of Commerce National Technical Information Service 5301 Shawnee Rd Alexandria, VA 22312

Telephone: (800) 553-6847 Facsimile: (703) 605-6900 E-Mail: orders@ntis.gov

Online order: <a href="https://classic.ntis.gov/help/order-methods/">https://classic.ntis.gov/help/order-methods/</a>



# **ABSTRACT**

Spray-formed materials have complex microstructures which pose challenges for microscale and mesoscale modeling. To constrain these models, experimental measurements of wave profiles when subjecting the material to dynamic compression are necessary. The use of a gas gun to launch a shock into a material is a traditional method to understand wave propagation and provide information of time-dependent stress variations due to complex microstructures. This data contains information on wave reverberations within a material and provides a boundary condition for simulation. Here we present measurements of the wavespeed and wave profile at the rear surface of tantalum, niobium, and a tantalum/niobium blend subjected to plate impact. Measurements of the Hugoniot elastic limit are compared to previous work and wavespeeds are compared to longitudinal sound velocity measurements to examine wave damping due to the porous microstructure.

# **ACKNOWLEDGEMENTS**

We thank Steven Dean, Keith Hodge, Lena Pacheco, and Josh Usher at the DICE facility for experimental support, and Sheri Payne and Dan Dolan for advice on measuring fiber delay times.

# **CONTENTS**

1.	Introduction	9
2.	Methods	11
	2.1. Sample and Target Preparation	11
	2.2. Experiment	12
3.	Diagnostic Cross-timing.	15
4.	Results/Discussion	19
5.	Conclusions	25
LI	ST OF FIGURES	
Fię	gure 1: Target design schematic for impactor (left) and target plate (right) used in transmitted wave experiments. 12-mm-thick sapphire windows back all samples (not shown). The	10
Fic	impactor diameter is illustrated with dashed green circle on target plategure 2: Raw VISAR data for Ta sample with 70 m/s VPF on shot DG646	
_	gure 3: Raw PDV signal (top) and spectrogram (bottom) for Ta sample on shot DG646	
	gure 4:Cross-timing data for ToA recorded on both PDV scopes. Time-mark on sample scop	
	was 18.3 ns later than on ToA scope.	
	gure 5: Ta wave profile data for shot DG646	
Fig	gure 6: Nb wave profile data for shot DG646. Light return for PDV was insufficient to extrac	
	velocity profile.	
	gure 7: Ta/Nb wave profile data for shot DG646	
	gure 8: Ta wave profile data for shot DG647. Light return for PDV was insufficient to extract velocity profile	21
_	gure 9: Nb wave profile data for shot DG647	21
Fig	gure 10: Nb wave profile data for shot DG646. Light return for VISAR was insufficient to extract velocity profile	22
Fig	gure 11: Impedance matching from Ta and Nb window velocities to peak pressure in Ta and Nb samples	23
1 19	ST OF TABLES	
	ble I: Measured thickness and density for samples tested on shots DG646 and DG647ble II: Lengths of probes used on DICE experiments	
	ible III: Internal delay measurements for PDV scopes in operation as of October 2021	
	ible IV: Measured PDV and VISAR motion relative to time marks on shot DG646 and required VISAR delay to match timed PDV results.	
Тэ	ible V: Impact velocity and impactor tilt for transmitted wave shots	
	ible VI: Transit time, wavespeed, peak stress, and HEL for samples tested on shots DG646 at DG647	nd
	D001/	2

This page left blank

# **ACRONYMS**

Abbreviation	Definition	
AR	Anti-reflective	
DICE	Dynamic Integrated Compression Experimental facility	
HEL	Hugoniot elastic limit	
PDV	Photonic Doppler velocimetry	
ToA	Time of arrival	
VISAR	Velocity interferometer system for any reflector	
VPF	Velocity per fringe	

### 1. INTRODUCTION

Cold spray deposition has been demonstrated to be an effective method to rapidly fabricate thick (>1 mm) coatings using a variety of materials[1-4]. Due to variability in the spray process, this method produces porous, underdense materials with a stochastic arrangement of pore shapes and sizes[5]. While such materials have been regularly studied using traditional techniques, such as tensile or indentation testing, the dynamic properties of spray-formed materials are largely unconstrained[6-14]. Due to the stochastic microstructure, application of a dynamic impulse triggers a series of compression and rarefaction waves which reflect off of material interfaces within the material. Understanding the propagation of these waves is highly complex and requires detailed modeling of the material microstructure[15-17].

To constrain codes to calculate the wave propagation, a variety of experimental data is required. This data includes measurement of the principal Hugoniot and spall strength, pressure-dependent pore compaction, and the wave profile transmitted into a known standard. Of particular interest is the behavior of high-strength materials which will resist compaction under dynamic loading. For this reason, we chose to study tantalum, a model BCC metal with no phase transitions over the pressure range of these experiments[18-24]. To understand whether material composition or porosity play the dominant role in wave propagation, a low-impedance refractory metal, niobium, and a blend of the two metals was also tested.

This report presents measurements of the wavespeed for shocks driven into the metal samples and wave profiles upon shock breakout into a sapphire window. To measure the wavespeed, cross-timing of the various photonic Doppler velocimetry (PDV) and velocity interferometer system for any reflector (VISAR) diagnostics at the Dynamic Integrated Compression Experimental (DICE) facility was required and diagnostic delays are given for the individual scopes and probes used. This report supplements work on cold-sprayed materials which was reported earlier[17].

### 2. METHODS

## 2.1. Sample and Target Preparation

Tantalum, niobium, and 70/30 tantalum/niobium blend samples were fabricated using the cold spray process. Sprayed samples were deposited as 3-4 mm thick layers onto 6061-T6 aluminum substrates, then cut into 19-mm-diameter discs using wire-electrical discharge machining and machined to a nominal thickness of 1.5 mm. Both samples from each type were taken from the same spray coupon. Final polishing produced ~1-mm-thick samples with flat and parallel surfaces. Details of the spray process and feedstocks used can be found in ref. [17]. Sample characterization for density and sound velocity and calculated elastic constants from measured values is also given in [17]. Measured thicknesses and densities calculated from mass and dimensions for the tested samples are given in Table I.

Table I: Measured thickness and density for samples tested on shots DG646 and DG647

Shot	Sample	Thickness [mm]	Density [g/cm³]	Relative Density	Sample
	Та	0.959±0.002	15.85±0.32	0.952	Та
DG646	Nb	1.023±0.002	8.04±0.16	0.938	Nb
	Ta/Nb	1.004±0.002	13.06±0.26	0.918	Ta/Nb
	Та	1.014±0.002	15.61±0.31	0.938	Та
DG647	Nb	0.976±0.002	7.96±0.16	0.929	Nb
	Ta/Nb	1.019±0.002	13.26±0.27	0.932	Ta/Nb

Samples were bonded to 19mm Dia × 12mm thick single-crystal sapphire windows oriented along the c-axis (Lattice Electro-Optics). The windows were coated with a 100-150 nm Al spot coating on the surface which mates to the sample, and an anti-reflective (AR) coating for 532 and 1550 nm on the back surface. A Romulan combination probe consisting of 4 flat-polished multimode fibers for 532 nm and 3 flat-polished singlemode fibers for 1550 nm was aligned to the spot coating on the sample/window interface. A 57mm Dia × 4.0mm thk c-axis sapphire plate was used as an impactor for these experiments.

The three-sample target plate was used for these experiments. In this configuration, three samples are mounted in the target plate in a triangular orientation and a time of arrival (ToA) probe was mounted in the center. In the event of no tilt, all three samples and the ToA probe are impacted simultaneously by the projectile. Calibrated shorting pins were installed into the target plate to measure the impact velocity and impactor tilt. A plane fit to the tilt pins was used to determine impactor tilt. One sample of each type was fielded on both shots. The projectile nosepiece had a relief void behind the sapphire impactor to allow for an overtaking wave to be launched into the sample. A schematic of the projectile and impactor is shown in Figure 1.

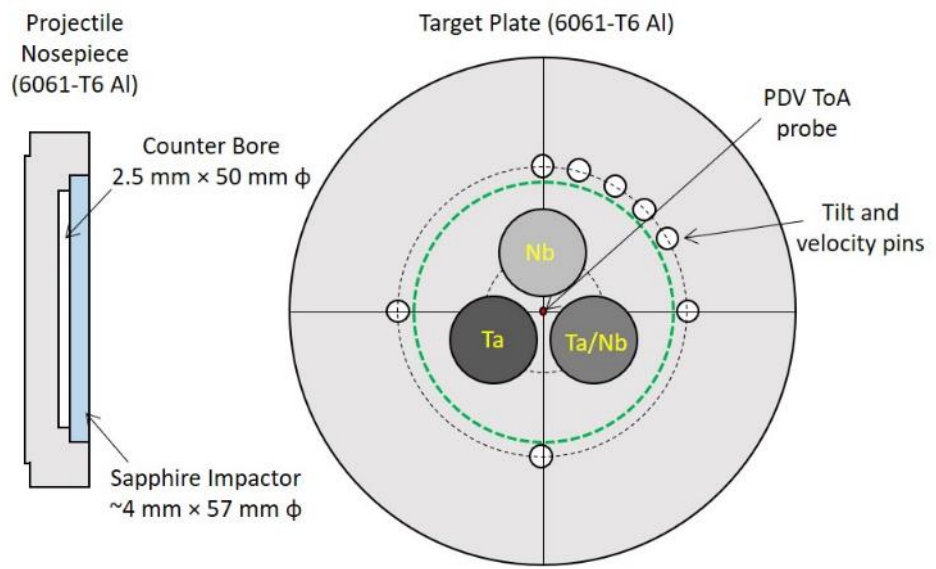


Figure 1: Target design schematic for impactor (left) and target plate (right) used in transmitted wave experiments. 12-mm-thick sapphire windows back all samples (not shown). The impactor diameter is illustrated with dashed green circle on target plate.

## 2.2. Experiment

Two shots were conducted on the single-stage gas gun at the DICE Facility at Sandia National Laboratories, Albuquerque. The DICE gas gun is a 3" bore gun with wrap-around breech capable of launching projectiles up to 400 m/s. Wave profiles at the sample-window interface were made with both VISAR[25, 26] and PDV[27, 28].

The DICE VISAR system uses a 532 nm Nd:YAG laser and records the return signal using a quadrature system. To mitigate potential ambiguities due to  $2\pi$  phase shifts, two distinct sensitivities (measured in velocity per fringe, VPF) were used. An example of the raw data is given in Figure 2. The VPFs chosen for these experiments were 70 and 90 m/s. To convert from apparent to true velocity, the VPF was divided by the refractive index of the sapphire window after applying the density correction given by Jones *et al*[29]. The stress transmitted into the sapphire window was determined from the sapphire Hugoniot from Jensen *et al*[30].

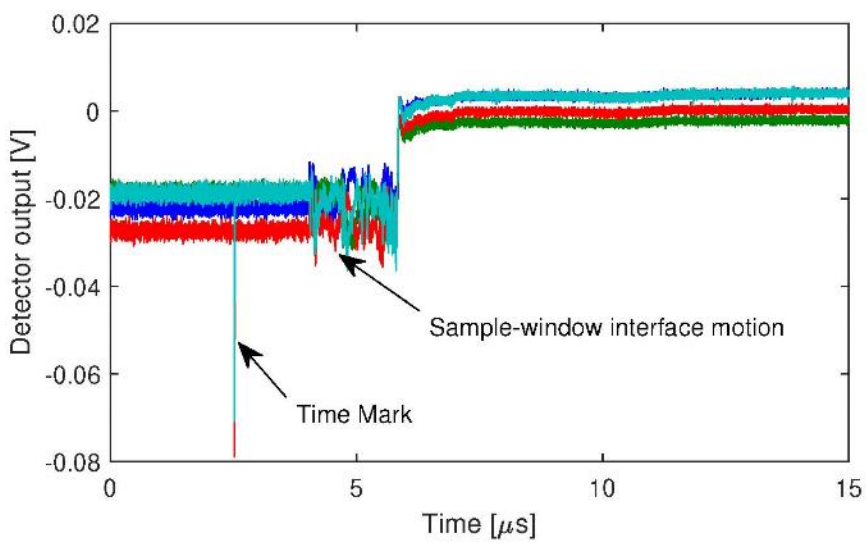


Figure 2: Raw VISAR data for Ta sample with 70 m/s VPF on shot DG646

The PDV measurement on the samples were made in the transmitted signal geometry, where separate send and receive fibers are used. Analysis of the raw spectrograms was done using SIRHEN[28]; an example signal and spectrogram is shown in Figure 3. On the first shot, DG646, the ToA probe fielded was a single-fiber collimated probe from Silicon Lightwave Technology, Inc. Being a collimated probe, this measurement had to be done in the reflected signal geometry, and was unable to be recorded on the same scope as the PDV signals from the back of the sample. On the second shot, DG647, this probe was replaced with a three-fiber pigtail from Ascentta Inc, and the signal was split to both PDV scopes and used to cross-time the PDV diagnostics.

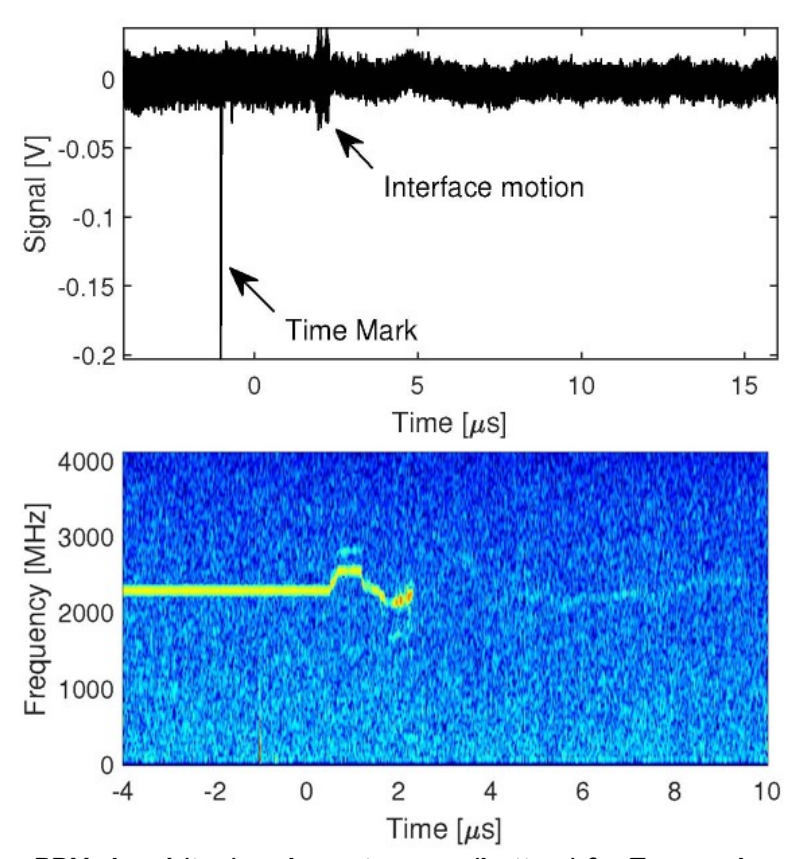


Figure 3: Raw PDV signal (top) and spectrogram (bottom) for Ta sample on shot DG646

### 3. DIAGNOSTIC CROSS-TIMING

To determine the velocity of the shock wave through the CS samples, it was necessary to cross-time the two PDV scopes and the VISAR system. The key elements to cross-timing the diagnostics are the length of the fiber runs from the diagnostic racks in the screen room to the patch panel on the gun, the length of fiber inside the gun, and internal delays built into the PDV scopes and VISAR digitizers. As the internal delay and fiber run do not change between shots, the only parameter which varies on a shot-to-shot basis is the length of fibers within the impact chamber. The lengths of various types of probes which are used on DICE shots are given in Table II.

Table II: Lengths of probes used on DICE experiments

Probe type	Probe use	Probe length [m]	Probe delay [ns]
Oz VISAR	Focusing VISAR	1.0	4.93
Romulan	Combo VISAR/PDV	1.0	4.87(V) / 4.90(P)
Romulan	Combo VISAR/PDV	2.5	12.18(V) / 12.24(P)
Silicon Lightwave	Collimated PDV	3.0	14.69
Coated Silicon Lightwave	Transmission ToA PDV	1.5	7.35
Coated Ascentta pigtail	Reflection ToA PDV	2.5	12.24

By knowing the probes used on a specific shot, the optical path difference can be calculated and the delay can be determined. All PDV probes used at DICE are fabricated from single-mode SMF-28 fibers (Corning Inc.) and have a refractive index of n=1.4682 at the 1550 nm wavelength used for PDV. The Romulan VISAR probes use a multi-mode pure silica fiber with refractive index of n=1.4607 at a wavelength of 532 nm. Oz VISAR probes use germanium doped fibers with pure silica cladding and a numerical aperture  $N_A=0.22$ . The index of these fibers can be found from  $N_A=0.22$ .

 $\sqrt{n_{\rm co}^2 - n_{\rm cl}^2}$  where subscripts  $\omega$  and  $\omega$  denote the core and cladding respectively. Using the refractive index of pure silica, this gives n=1.4772. Delay times for individual probes can be calculated as  $t_d = \frac{nl}{c}$ , where l is the fiber length and  $\varepsilon$  is the speed of light in vacuum, and are given in Table II.

On shot DG647, a coated Ascentta pigtail ToA was fielded with all three fibers operating as individual reflection ToA probes. The return signals were sent back to the same detector and read on channels 1-3. Internal delays for these channels were measured and are given in Table III. One of the output signals was combined with time mark #3 from the time-mark generator and read on a digital oscilloscope. A second signal was combined with time mark #2 and read on the same scope as the sample data, then branched over to the other scope using a 4-ft RG-58 coaxial cable with BNC cables. For the standard 50Ω RG-58 cable used, the quoted phase velocity is ¾c which gives a delay time of 6.10 ns. The third time mark (#1) was tied into the experimental data to confirm the difference between timing of the PDV scopes after the internal delay of the detectors.

Table III: Internal delay measurements for PDV scopes in operation as of October 2021

Scope	Channel	Delay
ToA (Blademaster)	1	42.94 ns
ToA (Blademaster)	2	39.70 ns
ToA (Blademaster)	3	47.26 ns
ToA (Blademaster)	4	47.10 ns
Sample ("Old")	All	39.42 ns

To relatively time the two PDV diagnostics, time mark #2 was used to relate the two scopes. Because it is branched simultaneously to both systems after the output from the PDV detectors, it is independent of the internal delay in the scopes, and only depends on the 4 ft additional cable length used to branch between the digitizers. Figure 4 shows the raw PDV signal from these two channels. Fitting between the time marks shown in the inset indicate that the ToA scope is 24.4 ns later than the sample scope. Accounting for the 4 ft cable connecting the scopes, timing for the ToA scope needs to be adjusted earlier by 18.3 ns to agree with the sample scope. Comparing the arrival time of time marks #1 and #3, time marks were identified with the ToA scope being 17.3 ns later than the sample scope. This delay agrees well with the value determined from branching the time mark. To estimate the uncertainty in the cross-timing, the average and range of both values can be used to give  $PDV_{ToA} = PDV_{sample} + 17.8 \pm 0.5ns$ .

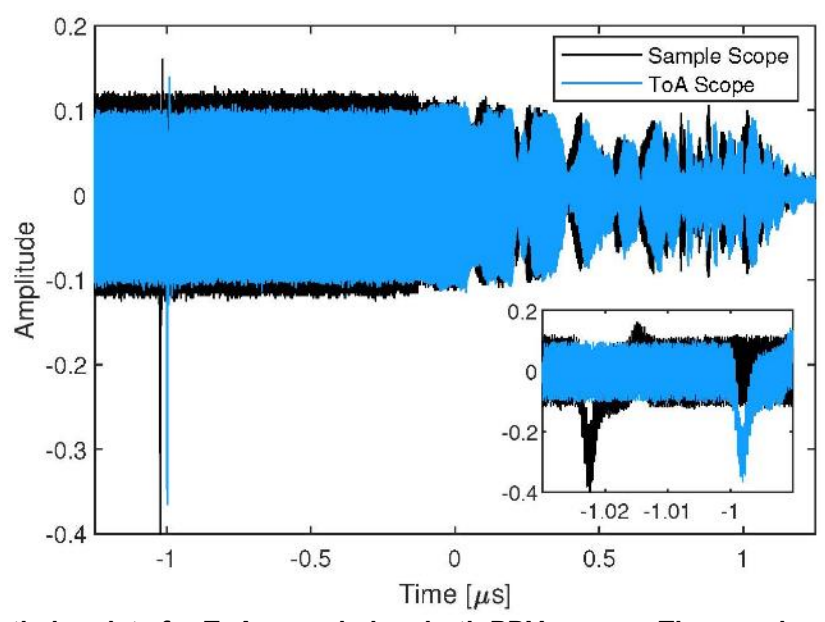


Figure 4:Cross-timing data for ToA recorded on both PDV scopes. Time-mark on sample scope was 18.3 ns later than on ToA scope.

To cross-time the VISAR diagnostic to PDV, the time mark was used in conjunction with experimental data from the back of the sample. Because PDV and VISAR were observing the same sample, the onset of motion coincides for both diagnostics and the timing of VISAR was adjusted to match the timed result for both shots. As the time marks for VISAR and PDV do not account for detector delays, a time shift for the data based on the VISAR and PDV time marks is used. In these

experiments, no absolute timing is considered due to inherent jitter in a gun experiment. As shown for the Ta sample in Figures 2 and 3, time marks occur at 2.5225  $\mu$ s for VISAR and -1.0303  $\mu$ s for PDV, and motion begins at 4.0454  $\mu$ s and 0.5028  $\mu$ s, respectively. Subtracting the time marks from the data sets finds that the onset of motion is 1.5229  $\mu$ s after the time mark in VISAR and 1.5331  $\mu$ s later in PDV. As the delay  $\tau$  inherent to VISAR for a 70 m/s velocity sensitivity is >3 ns and the path difference is <0.5 ns, the internal delay for the VISAR channel shown can be assumed to be the same as that for PDV. This exercise was repeated for all 6 VISAR channels used and values are given in Table IV.

Table IV: Measured PDV and VISAR motion relative to time marks on shot DG646 and required VISAR delay to match timed PDV results.

VISAR Channels	PDV Motion	VISAR Motion	Delay
T15	1.5331 <b>μ</b> s	1.5229 <b>μ</b> s	<1.0 ns
T16	1.5331 µs	1.5222 <b>μ</b> s	<1.0 ns
T17	1.8031 µs	1.7998 <b>μ</b> s	3.3 ns
T18	1.8031 µs	1.8076 μs	-4.5 ns
T19	1.5886 <b>μ</b> s	1.5820 <b>μ</b> s	6.6 ns
T20	1.5886 <b>µ</b> s	1.5819 <b>μ</b> s	6.7 ns

### 4. RESULTS/DISCUSSION

The target velocities for these shots were 160 and 227 m/s to match previous work done on air-plasma-sprayed materials[15]. Measured velocities from the shorting pins and calculated tilt are given in Table V. On each shot, VISAR and PDV data were collected on all three samples. Due to the thickness of the windows, light return for the Romulan probes was low and some data was lost on some samples. On all samples usable data was returned for either VISAR or PDV.

Table V: Impact velocity and impactor tilt for transmitted wave shots

Shot	Impact velocity	Tilt
DG646	242.2±3.7 m/s	8.6 mrad
DG647	171.3±0.8 m/s	14.4 mrad

Velocity traces were obtained at the interface of the sample and sapphire window. These traces showed an initial sharp rise in velocity, a kink at the Hugoniot Elastic Limit (HEL), and a further increase to a plateau at approximately constant velocity. The initial sharp rise is due to an elastic precursor in the shocked samples, which is followed by the plastic wave which further compresses the sample and is transmitted into the window. Window velocities for the tested samples are given in Figures 5-10.

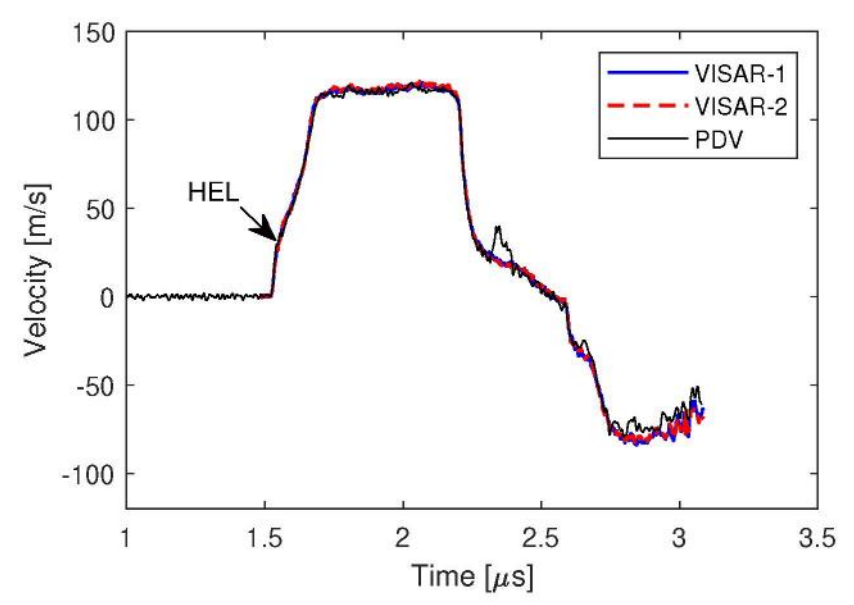


Figure 5: Ta wave profile data for shot DG646.

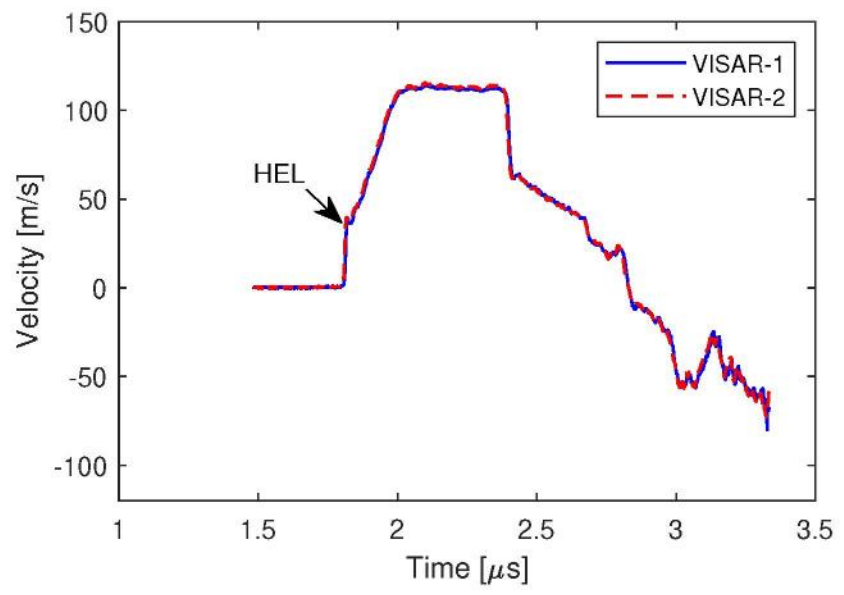


Figure 6: Nb wave profile data for shot DG646. Light return for PDV was insufficient to extract velocity profile.

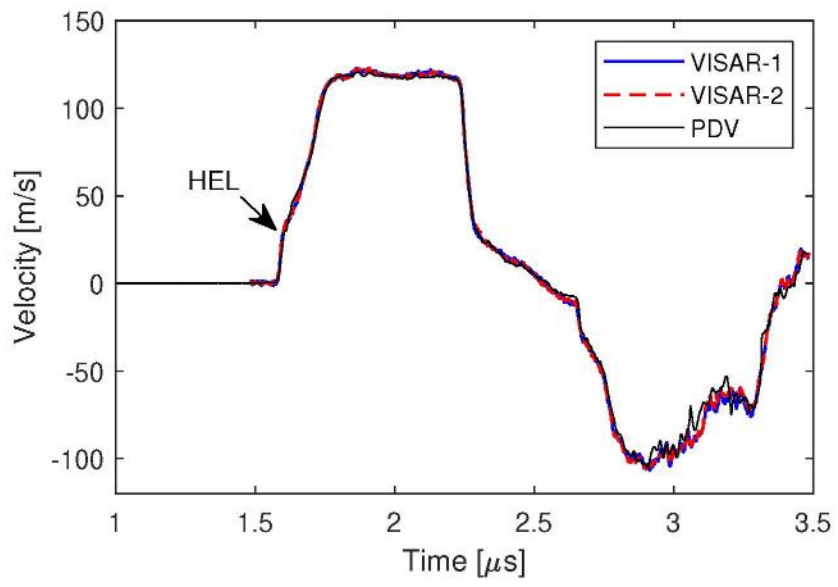


Figure 7: Ta/Nb wave profile data for shot DG646.

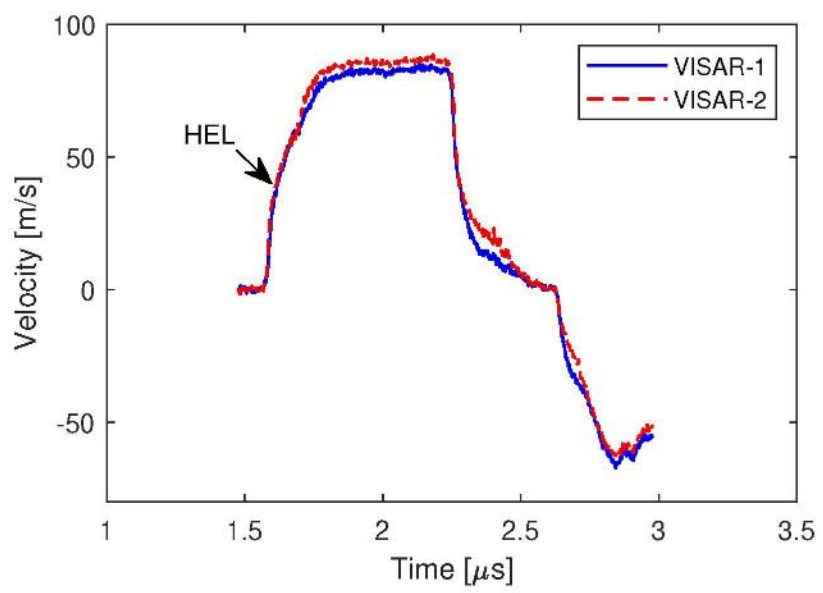


Figure 8: Ta wave profile data for shot DG647. Light return for PDV was insufficient to extract velocity profile

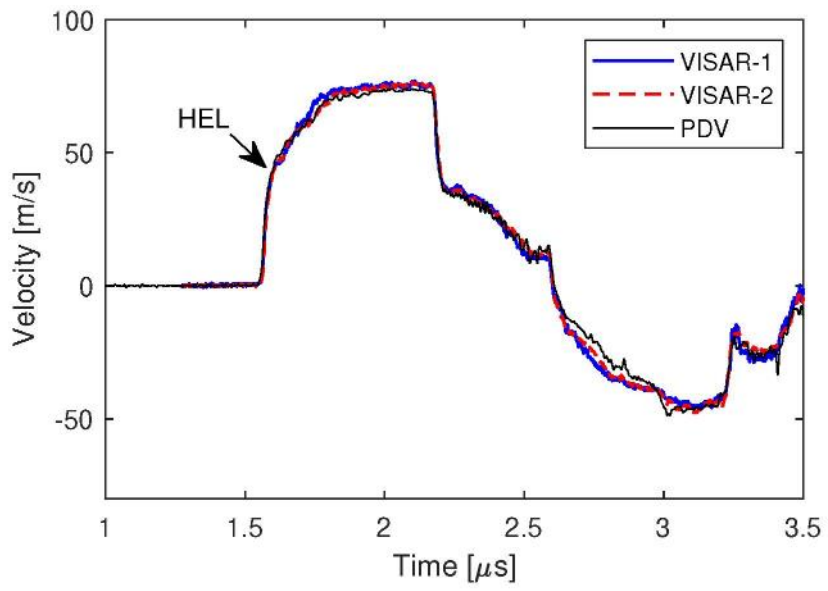


Figure 9: Nb wave profile data for shot DG647.

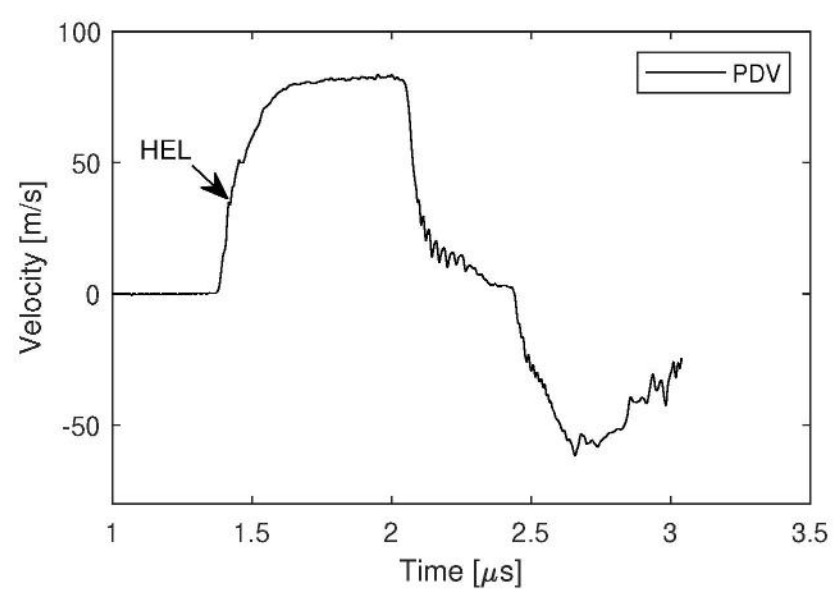


Figure 10: Nb wave profile data for shot DG646. Light return for VISAR was insufficient to extract velocity profile

Similar to the spall experiments described by Branch, McCoy, and Vackel[17], variation in the wave profile is observed at the peak velocities shown in Figures 5-10. This is related to the heterogeneous structure and wave reverberations within the sample. Because voids are stochastically dispersed throughout the sample, the shock front within the samples have significant spatial variation and wave propagation within the sample is complex. As these waves propagate into the sapphire window, they are manifested as small variations to the shock velocity. The existence of these variations throughout the entire duration of the semi-constant peak stress indicates that damping of acoustic waves within the sample takes a period greater than a round-trip transit time within the sample.

By assuming a reflected Hugoniot approximation for the release from the sample into the sapphire window, the HEL and peak stress can be determined for these samples. An example impedance matching diagram for the higher-pressure Ta and Nb samples and the sapphire window is shown in Figure 11. The measured Hugoniot from [17] indicates that over the range of pressures in these experiments, Ta has very similar impedance to sapphire, whereas that for Nb is noticeably less such that a moderate-strength reflected shock is driven into the Nb from the sapphire window. In addition to the HEL, the wavespeed through the sample and peak stress can be determined from the shock wave transit time. By conducting the exercise to cross-time the diagnostics, as described in Section 3, the impact time measured with the ToA probe and the shock breakout time can be directly compared to extract a transit time. Then by using the measured thicknesses from Table I the average shock velocity through the sample can be determined. The Hugoniot stress as a function of particle velocity is given in [17]. Values of the elastic shock velocity ( $U_S^{el}$ ), peak stress ( $\sigma$ ), and HEL are given in Table VI.

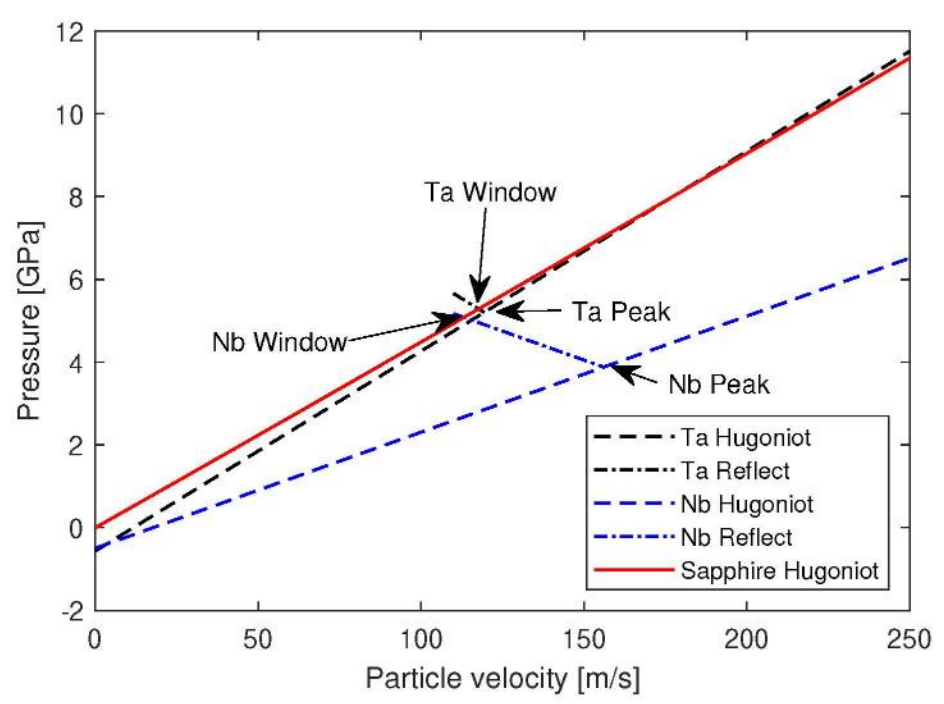


Figure 11: Impedance matching from Ta and Nb window velocities to peak pressure in Ta and Nb samples

Table VI: Transit time, wavespeed, peak stress, and HEL for samples tested on shots DG646 and DG647

Shot	Sample	Transit time [µs]	$U_S^{el}$ [mm/ $\mu$ s]	σ [GPa]	HEL [GPa]
	Та	0.2034±0.0081	4.64±0.18	5.20±0.18	0.66±0.18
DG646	Nb	0.1957±0.0078	3.11±0.14	3.88±0.14	1.10±0.14
	Ta/Nb	0.2256±0.0090	4.10±0.17	4.93±0.17	1.17±0.17
	Та	0.4024±0.16	2.52±0.12	3.64±0.18	0.99±0.18
DG647	Nb	0.4002±0.0017	2.44±0.12	2.46±0.15	1.07±0.15
	Ta/Nb	0.3710±0.0015	2.75±0.11	2.91±0.17	1.30±0.17

The measured elastic wavespeeds do not agree with the longitudinal sound speed measurements presented in [17]. On DG646 with impact at ~240 m/s, the measured wavespeed for Ta is ~1 mm/µs greater than the longitudinal velocity. This would be expected for higher impact pressures where the wavespeed will increase with compressed density. However, in the weak shock limit, the expected wavespeed would be similar to the longitudinal velocity. The only sample where the wavespeed is similar to the longitudinal velocity is for the Nb sample on shot DG646. The wavespeed for the Ta/Nb blend agrees well with a 70/30 linear combination of the measured values for the individual species, which is in line with expectations.

On shot DG647, the measured wavespeeds are suppressed compared to the longitudinal sound velocity, with values for all three samples being 80-90% of the previous value. This is in better agreement with expectations for this work as the weak shock compresses pores within the sprayed

sample and dissipates energy through this process. Values for the individual species are similar, but the measured value for the blend is 10% greater than the individual results. This may be related to the increased HEL as a stronger elastic wave would more efficiently compact pores and be transmitted through the sample.

Wavespeeds presented in Table VI may not accurately represent the true elastic shock velocity in the material. While the uncertainties given have been calculated using a Monte Carlo method to incorporate random errors in impact velocity, impactor tilt, sample and ToA height relative to the target plate, and detector resolution, an unknown systematic uncertainty may be present. The mounting of the ToA probe in the target plate is done with a small amount of glue at the back of the probe after dropping the probe into the bore so it sits against a flat surface. Examination of target plates used for a different series has shown that it is possible for the ToA probes to move within the target plate when pulling vacuum in the impact chamber. Additionally, free-streaming gas ahead of the impactor has been demonstrated to apply sufficient force to displace the ToA probes prior to impact. This would result in measured impact times being systematically late, which would artificially inflate the measured wavespeeds. New methods for impact measurement are under discussion and will be implemented for future series at the DICE facility.

HELs measured on these shots agree well with the values measured on the spall shots in Ref. [17] for both the Nb and Ta/Nb blend. These results are consistent for both shots and show no statistically significant dependence on the peak stress. The previous values are also within the uncertainty determined in this work. Uncertainty in the previous work would be similar due to the nature of the experiments. The pure Ta shows a significant difference in the HEL. In these experiments, a value of 0.66 GPa was identified when shocked to a peak stress of 5.20 GPa, and a value of 0.99 GPa was measured for a peak stress of 3.64 GPa. The previously reported value of 1.57 GPa was achieved with a peak stress similar to DG647, so further work would be necessary to constrain a true HEL for the pure Ta.

### 5. CONCLUSIONS

Transmitted wave shock experiments were carried out for cold-sprayed deposits of tantalum, niobium and a 70/30 tantalum-niobium blend. Wavespeeds were measured for shocks launched by the impact of 171 m/s and 242 m/s sapphire flyer plates. Nb and Ta/Nb wavespeeds from the 242 m/s experiment agreed with previously reported longitudinal sound velocities, whereas the Ta wavespeed was significantly greater than the sound velocity. At an impact velocity of 171 m/s, wavespeeds were suppressed relative to the sound velocity by wave interactions between splats and voids within the material. The Hugoniot elastic limit was measured for all three materials and the Nb and Ta/Nb were found to agree with previously reported results, whereas the Ta HEL has a significant variation on a shot-to-shot basis. Differences between the Ta HEL in this work and the previous work may be related to process variation between sprayed coupons, however the discrepancy between the two samples tested in this work cannot be explained in this manner.

Wavespeed measurements identified a potential systematic issue with ToA measurements at the DICE facility. Because the probe offset is not necessarily fixed when pulling vacuum or being acted upon by air streaming ahead of the impactor, it does not provide a reliable measurement of the impact time. Additional work is required to redesign the target plate and probe setup for accurate measurements of the impact time.

## **REFERENCES**

- [1] T. Van Steenkiste and D. W. Gorkiewicz, "Analysis of tantalum coatings produced by the kinetic spray process," *Journal of Thermal Spray Technology*, journal article vol. 13, no. 2, pp. 265-273, June 01 2004, doi: 10.1361/10599630419418.
- [2] K. Y. Wenya Li, Shuo Yin, Xiawei Yang, Yaxin Xu, Rocco Lupoi, "Solid-state additive manufacturing and repairing by cold spraying: A review," *J. Mater. Sci. Technol.*, vol. 34, no. 3, pp. 440-457, 2018-03-20 2018, doi: 10.1016/j.jmst.2017.09.015.
- [3] M. Vaezi, P. Drescher, and H. Seitz, "Beamless Metal Additive Manufacturing," *Materials*, vol. 13, no. 4, p. 922, 2020. [Online]. Available: <a href="https://www.mdpi.com/1996-1944/13/4/922">https://www.mdpi.com/1996-1944/13/4/922</a>.
- [4] R. N. Raoelison *et al.*, "Cold gas dynamic spray technology: A comprehensive review of processing conditions for various technological developments till to date," *Additive Manufacturing*, vol. 19, pp. 134-159, 2018/01/01/ 2018, doi: https://doi.org/10.1016/j.addma.2017.07.001.
- [5] F. S. da Silva, N. Cinca, S. Dosta, I. G. Cano, J. M. Guilemany, and A. V. Benedetti, "Effect of the Outer Layer of Al Coatings Deposited by Cold Gas Spray on the Microstructure, Mechanical Properties and Corrosion Resistance of the AA 7075-T6 Aluminum Alloy," *Journal of Thermal Spray Technology*, vol. 29, no. 5, pp. 1040-1053, 2020/06/01 2020, doi: 10.1007/s11666-020-01023-8.
- [6] P. Cavaliere and A. Silvello, "Mechanical properties of cold sprayed titanium and nickel based coatings," *Surface Engineering*, vol. 32, no. 9, pp. 670-676, 2016, doi: 10.1179/1743294415y.0000000080.
- [7] S. I. Imbriglio *et al.*, "Adhesion strength of titanium particles to alumina substrates: A combined cold spray and LIPIT study," *Surface & Coatings Technology*, vol. 361, pp. 403-412, Mar 2019, doi: 10.1016/j.surfcoat.2019.01.071.
- [8] D. M. Jafarlou, C. Walde, V. K. Champagne, S. Krishnamurty, and I. R. Grosse, "Influence of cold sprayed Cr3C2-Ni coating on fracture characteristics of additively manufactured 15Cr-5Ni stainless steel," *Materials & Design*, vol. 155, pp. 134-147, Oct 2018, doi: 10.1016/j.matdes.2018.05.063.
- [9] K. E. Machethe, A. P. I. Popoolab, D. I. Adebiyi, and O. S. I. Fayomi, "Influence of SiC-Ti/Al on the Microstructural and Mechanical Properties of Deposited Ti-6V-4A1 Alloy with Cold Spray Technique," in *International Conference on Sustainable Materials Processing and Manufacturing*, vol. 7, T. C. Jen, W. Chiu, E. Akinlabi, and H. S. Chen Eds., (Procedia Manufacturing, 2016, pp. 549-555.
- [10] N. B. Maledi, O. P. Oladijo, I. Botef, T. P. Ntsoane, A. Madiseng, and L. Moloisane, "Influence of cold spray parameters on the microstructures and residual stress of Zn coatings sprayed on mild steel," *Surface & Coatings Technology*, vol. 318, pp. 106-113, May 2017, doi: 10.1016/j.surfcoat.2017.03.062.
- [11] A. Moridi, S. M. Hassani-Gangaraj, S. Vezzu, L. Trsko, and M. Guagliano, "Fatigue behavior of cold spray coatings: The effect of conventional and severe shot peening as pre-/post-treatment," *Surface & Coatings Technology*, vol. 283, pp. 247-254, Dec 2015, doi: 10.1016/j.surfcoat.2015.10.063.
- [12] A. Silvello, P. Cavaliere, A. Rizzo, D. Valerini, S. D. Parras, and I. G. Cano, "Fatigue Bending Behavior of Cold-Sprayed Nickel-Based Superalloy Coatings," *Journal of Thermal Spray Technology*, vol. 28, no. 5, pp. 930-938, Jun 2019, doi: 10.1007/s11666-019-00865-1.

- [13] J. R. Tang *et al.*, "Influence of feedstock powder on microstructure and mechanical properties of Ta cold spray depositions," *Surface & Coatings Technology*, vol. 377, Nov 2019, Art no. Unsp 124903, doi: 10.1016/j.surfcoat.2019.124903.
- [14] Z. P. Zhao *et al.*, "Influence of annealing on the microstructure and mechanical properties of Ti/steel clad plates fabricated via cold spray additive manufacturing and hot-rolling," *Materials Science and Engineering a-Structural Materials Properties Microstructure and Processing*, vol. 775, Feb 2020, Art no. 138968, doi: 10.1016/j.msea.2020.138968.
- [15] N. W. Moore, G. R. Chantler, A. Vackel, J. L. Wise, R. Pokharel, and D. Brown, "Stochastic shock observations from plate impact of porous refractory metals," Sandia National Laboratories, Albuquerque, NM, SAND2019-10376, 2019.
- [16] C. A. McCoy, N. W. Moore, and A. Vackel, "Microstructural Changes to Thermally Sprayed Materials Subjected to Dynamic Compression," Sandia National Laboratories, Albuquerque, NM, SAND2020-10133, 2020.
- [17] B. A. Branch, C. A. McCoy, and A. Vackel, "Impact Response of Cold Spray Deposited Materials," Sandia National Laboratories, Albuquerque, NM, SAND2020-10575, 2020.
- [18] J. Brown and J. Shaner, "Rarefaction velocities in shocked tantalum and the high-pressure melting point," Texas A and M Univ., College Station (USA); Los Alamos National Lab., NM (USA), 1983.
- [19] J. L. Brown, C. S. Alexander, J. R. Asay, T. J. Vogler, D. H. Dolan, and J. L. Belof, "Flow strength of tantalum under ramp compression to 250 GPa," *Journal of Applied Physics*, vol. 115, no. 4, p. 043530, 2014.
- [20] J.-P. Davis, J. L. Brown, M. D. Knudson, and R. W. Lemke, "Analysis of shockless dynamic compression data on solids to multi-megabar pressures: Application to tantalum," *Journal of Applied Physics*, vol. 116, no. 20, p. 204903, 2014.
- [21] J. L. Ding, J. R. Asay, and T. Ao, "Modeling of the elastic precursor behavior and dynamic inelasticity of tantalum under ramp wave loading to 17 GPa," *Journal of Applied Physics*, vol. 107, no. 8, p. 083508, 2010, doi: 10.1063/1.3373388.
- [22] D. R. Jones, S. J. Fensin, B. G. Ndefru, D. T. Martinez, C. P. Trujillo, and G. T. GrayIII, "Spall fracture in additive manufactured tantalum," *Journal of Applied Physics*, vol. 124, no. 22, p. 225902, 2018, doi: 10.1063/1.5063930.
- [23] A. C. Mitchell and W. J. Nellis, "Shock Compression of Aluminum, Copper, and Tantalum," *J. Appl. Phys.*, vol. 52, no. 5, pp. 3363–3374, 1981.
- [24] R. G. Kraus *et al.*, "Melting of Tantalum at Multimegabar Pressures on the Nanosecond Timescale," *Physical Review Letters*, vol. 126, no. 25, p. 255701, 06/24/2021, doi: 10.1103/PhysRevLett.126.255701.
- [25] L. M. Barker and R. E. Hollenbach, "Laser Interferometer for Measuring High Velocities of Any Reflecting Surface," *J. Appl. Phys.*, vol. 43, no. 11, pp. 4669–4675, 1972, doi: <a href="http://dx.doi.org/10.1063/1.1660986">http://dx.doi.org/10.1063/1.1660986</a>.
- [26] L. M. Barker and K. W. Schuler, "Correction to the Velocity-Per-Fringe Relationship for the VISAR Interferometer," *J. Appl. Phys.*, vol. 45, no. 8, pp. 3692–3693, 1974.
- [27] D. H. Dolan and S. C. Jones, "Push-pull analysis of photonic Doppler velocimetry measurements," *Review of Scientific Instruments*, vol. 78, no. 7, p. 076102, 2007, doi: 10.1063/1.2754405.
- [28] T. Ao and D. H. Dolan, "SIRHEN: a data reduction program for photonic Doppler velocimetry measurements," Sandia National Laboratories, SAND2010-3628, 2010.

- [29] S. C. Jones, M. C. Robinson, and Y. M. Gupta, "Ordinary refractive index of sapphire in uniaxial tension and compression along the c axis," *Journal of Applied Physics*, vol. 93, no. 2, pp. 1023-1031, 2003, doi: 10.1063/1.1530716.
- [30] B. J. Jensen, D. B. Holtkamp, P. A. Rigg, and D. H. Dolan, "Accuracy limits and window corrections for photon Doppler velocimetry," *Journal of Applied Physics*, vol. 101, no. 1, p. 013523, 2007, doi: 10.1063/1.2407290.

# **DISTRIBUTION**

## Email—Internal

Name	Org.	Sandia Email Address
Shawn Pautz	1341	sdpautz@sandia.gov
Aaron Olson	1341	aolson@sandia.gov
Nathan Moore	1344	nwmoore@sandia.gov
James Carleton	1443	jbcarle@sandia.gov
Mikhail Mesh	1553	mmesh@sandia.gov
Bill Scherzinger	1558	wmscher@sandia.gov
Brittany Branch	1646	babranc@sandia.gov
Chad McCoy	1646	camccoy@sandia.gov
Steven Dean	1647	swdean@sandia.gov
Andrew Vackel	1834	avackel@sandia.gov
Corbett Battaile	1864	ccbatta@sandia.gov
Theron Rodgers	1864	trodger@sandia.gov
Technical Library	01977	sanddocs@sandia.gov

This page left blank

This page left blank



Sandia National Laboratories is a multimission laboratory managed and operated by National Technology & Engineering Solutions of Sandia LLC, a wholly owned subsidiary of Honeywell International Inc. for the U.S. Department of Energy's National Nuclear Security Administration under contract DE-NA0003525.